

Article

A Sustainable Multistage Process for Immobilizing Bioactive Compounds on Layered Double Hydroxides

Serena Coiai ^{1,*}, Elisa Passaglia ¹, Alice Telleschi ¹, Werner Oberhauser ², Maria-Beatrice Coltelli ³
and Francesca Cicogna ¹

¹ National Research Council-Institute for the Chemistry of OrganoMetallic Compounds (CNR-ICCOM), Pisa Secondary Side, Via Moruzzi 1, 56124 Pisa, Italy; elisa.passaglia@pi.iccom.cnr.it (E.P.); alitelleschi@gmail.com (A.T.); francesca.cicogna@pi.iccom.cnr.it (F.C.)

² National Research Council-Institute for the Chemistry of OrganoMetallic Compounds (CNR-ICCOM), Via Madonna del Piano 10, 50019 Sesto Fiorentino, Italy; woberhauser@iccom.cnr.it

³ Department of Civil and Industrial Engineering, University of Pisa, Largo L. Lazzarino 1, 56122 Pisa, Italy; maria.beatrice.coltelli@unipi.it

* Correspondence: serena.coiai@pi.iccom.cnr.it; Tel.: +39-050-3152556

Abstract: Hybrid systems with antioxidant properties have been developed by integrating bioactive compounds derived from plant resources with layered double hydroxides (LDHs). Anion exchange has been used to substitute intercalated nitrate anions in Mg-Al LDH with carboxylate anions derived from trans-ferulic acid, rosmarinic acid, and 18 β -glycyrrhetic acid. These organic compounds are known for their powerful antioxidant, anti-inflammatory and antimicrobial properties and are highly suitable for cosmetics, biomedicine, and food packaging. To enhance sustainability, a multistage procedure has been developed with the aim of recovering unexchanged carboxylate anions from residual reaction water, ensuring an environmentally friendly and easily scalable preparation process. The process, adapted for each of the three molecules, allows the production of a consistently high-quality hybrid product containing an organic fraction ranging from 10 to 48% by weight, depending on the specific molecule used. The immobilization of organic compounds has occurred either within the layers of LDH through intercalation or on the external surface through adsorption. Good antioxidant capacity has been exhibited by these powdered hybrid systems, as assessed through both the DPPH and linoleic acid/ β -carotene tests. Sustainable production practices are enabled by this innovative approach, which also opens avenues for the development of advanced materials for diverse applications across various industries.

Keywords: layered double hydroxides; trans-ferulic acid; rosmarinic acid; 18 β -glycyrrhetic acid; multistage sustainable process; antioxidant test



Citation: Coiai, S.; Passaglia, E.; Telleschi, A.; Oberhauser, W.; Coltelli, M.-B.; Cicogna, F. A Sustainable Multistage Process for Immobilizing Bioactive Compounds on Layered Double Hydroxides. *Cosmetics* **2024**, *11*, 52. <https://doi.org/10.3390/cosmetics11020052>

Academic Editor: Vasil Georgiev

Received: 31 January 2024

Revised: 8 March 2024

Accepted: 14 March 2024

Published: 2 April 2024



Copyright: © 2024 by the authors. Licensee MDPI, Basel, Switzerland. This article is an open access article distributed under the terms and conditions of the Creative Commons Attribution (CC BY) license (<https://creativecommons.org/licenses/by/4.0/>).

1. Introduction

Layered double hydroxides (LDHs) are a class of inorganic layered materials characterized by positively charged ordered metal hydroxide layers that can immobilize diverse molecules in the interlayer space or on their surface. Known for their anion exchange capabilities, compositional flexibility, and high surface-to-volume ratio, LDHs are gaining significant attention across various technological sectors, including cosmetics and pharmaceuticals [1–5].

LDHs can be employed as nanocarriers for various active molecules in topical delivery due to their distinctive features, such as biocompatibility, stability, and high encapsulation capacity for actives [6]. They also stand out for enhancing the preservation of biomolecules, facilitating controlled release, and increasing bioavailability. Furthermore, LDHs are regarded as eco-friendly due to their inherent biocompatibility, use of water-based synthesis methods, and low production of hazardous effluents when incorporating naturally bioac-

tive molecules as modifiers [7]. Additionally, they are economically advantageous, utilizing readily accessible and cost-effective starting materials.

Numerous studies have highlighted the potential of LDHs as functional agent carriers and there are numerous examples in the literature related to the preparation and characterization of these host–guest bioactive systems [3]. In general, modified LDHs can be prepared by three methodologies: anion exchange, a versatile procedure allowing control of the final composition and structure, co-precipitation of inorganic salt precursors in a basic medium, and calcination followed by reconstruction. These different synthetic approaches enable a flexible strategy for obtaining modified LDHs [8]. Furthermore, LDHs show high porosity and surface basicity, facilitating interactions with various molecules and pH-dependent biodegradation. Intriguingly, modified LDHs play a role in slowing down and controlling the release of immobilized functional molecules, protecting them from thermal, oxidative, and photoinduced degradation. These characteristics make LDHs compelling additives in drug delivery systems and cosmetics applications [9]. Indeed, the low or negligible toxicity of LDHs, coupled with their capacity to deliver and control the release of active molecules while safeguarding them from degradation, contributes to extend the service life and applicability of the final products in both applications.

Skin care products have seen an increased presence in the market in recent years due to the growing need to maintain healthy and protected skin. Recently, to improve different aspects such as effectiveness, duration, and consistency of skin care products, formulations contain various nanoclay systems, with particular attention to those based on modified LDHs because, in addition to all the positive characteristics described earlier, they can deliver and protect antioxidants, UV filters, and nutrient molecules from oxidation [3,6,10]. Furthermore, the positive surface charge of LDHs allows for easy penetration into the cell membrane, significantly improving intracellular delivery, and the colloidal characteristics of LDHs suggest their use as structural ingredients in topical formulations, as thickeners, emulsifiers, and gelling agents.

Several examples are reported in the literature, such as the immobilization of azelaic acid in LDH, a dicarboxylic acid successfully used in many cosmetic and dermatological formulations to treat acne, rosacea, skin spots, and hair loss. This immobilization in LDH prevents the undesirable aggregation typical of free acid, allowing for a uniform dispersion of azelaic acid on the skin, while the anionic clay provides a protective and eudermic action [11]. The synergistic effectiveness of host–guest systems in skin care product formulations is also evident in the case of the intercalation of folic acid used to treat aged and photodamaged skin. The intercalation of folic acid in LDH not only improves the UV stability of folic acid and extends its acidic photoprotection but also positively influences the rheological properties of the formulation [12].

Similarly, cinnamic, ferulic, and caffeic acids, known for their bioactive properties, have been effectively intercalated into LDHs, resulting in hybrid systems where the organic molecules are protected and released in a controlled manner [13–18]. Trans-ferulic acid (FA-H), abundant in whole grains, botanical sources, and medicinal essences, has numerous therapeutic benefits, including antioxidant, antimicrobial, and anti-inflammatory effects and the ability to absorb UV light, making it a promising cosmetic ingredient [19]. However, although FA-H is already used as an active ingredient in skin care products and sunscreens, its use is limited by its poor stability after exposure to air and light. Advantages in terms of increased stability against degradation and controlled release have been achieved by intercalating it between the layers of LDH. Rosmarinic acid (RA-H), extracted from various plants, including sage, rosemary, and lemon balm, possesses antioxidant properties, antimicrobial activity, and anti-inflammatory and cytotoxic effects [20–22]. In our research group, we have recently demonstrated the possibility of intercalating RA-H between the layers of LDH and benefiting from the antimicrobial and antioxidant properties of the immobilized molecule by dispersing the hybrid system in polymeric matrices [23–25]. 18 β -Glycyrrhetic acid (GA-H), derived from glycyrrhizic acid, which is the main component of licorice root, is known for its antimicrobial and anti-inflammatory activity, as well

as for other properties such as its antiulcer and antidiabetic capacity, and has already found applications in the pharmaceutical and cosmetic sectors [26]. Its protection in chitin nanofibril–nanolignin complexes was investigated to obtain nanostructured microparticles combining thermal resistance with anti-microbial and anti-inflammatory properties [27]. In particular, its use in molded beauty films [28] or electro-spun pullulan tissues [29], both used for beauty masks, resulted in benefits for the skin [30]. Recently, GA-H immobilized in LDH and dispersed in a PLA/PBS mixture [25] has opened possibilities in active packaging, while encapsulation in PLGA nanoparticles has shown greater efficacy than pure acid, which suggests a potential use in targeted antimicrobial therapies [31].

From the previous discussion, it is evident that the immobilization of active molecules in LDH presents potential interest in cosmetic formulations [32]. Furthermore, considering the “green” nature of LDHs, their modification with natural biomolecules will produce ecological additives for cosmetic formulations. In addition, the process can add value to discarded products if the active biomolecules are extracted from agri-food wastes. Accordingly, in this work FA-H, RA-H, and GA-H (Figure 1) have been selected as bioactive molecules because of their unique functional properties and because they all contain a carboxylic acid group that can be deprotonated. This allows them to be intercalated in between LDH layers through anion exchange, leading to nanostructured host–guest systems. Furthermore, the natural origin and accessibility of these molecules from agri-food chain wastes constitutes an additional motivation for their study.

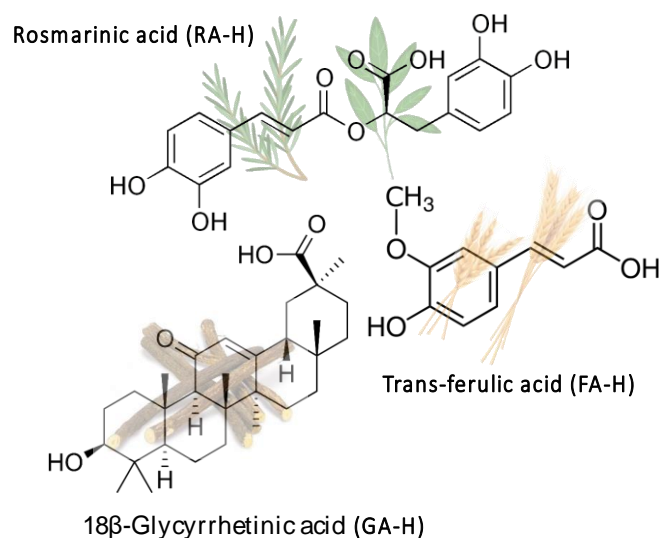


Figure 1. Molecular structures of trans-ferulic acid (FA-H), rosmarinic acid (RA-H), and 18β-glycyrrhetic acid (GA-H), with examples of their plant sources shown in transparency.

As previously discussed, one of the synthesis methods for producing modified LDHs is the anion exchange process (Figure 2), which exploits the ability of certain LDHs to exchange interlayer anions with other organic anions.

Typically, this process generates a water residue that still contains a relatively high quantity of active products, which cannot be immobilized in the initial phase. Accordingly, this study aims to develop a process that, through multiple stages of anion exchange, focuses on the complete recovery of organic anions. This approach is crucial for optimizing the yield of the hybrid product, minimizing the loss of active molecules, which originate from natural sources and have been obtained through demanding extraction processes. The water consumption reduction, possible because of the reuse of the residual water, can further improve the sustainability of the whole process.

In this study, we applied the multistage process of LDH modification to immobilize FA-H, RA-H, and GA-H. Specifically, we investigated optimization methods for each bioactive molecule, characterizing the hybrid product and reaction waters at different process stages. We also assessed the functional hybrid products’ structural and antioxidant properties.

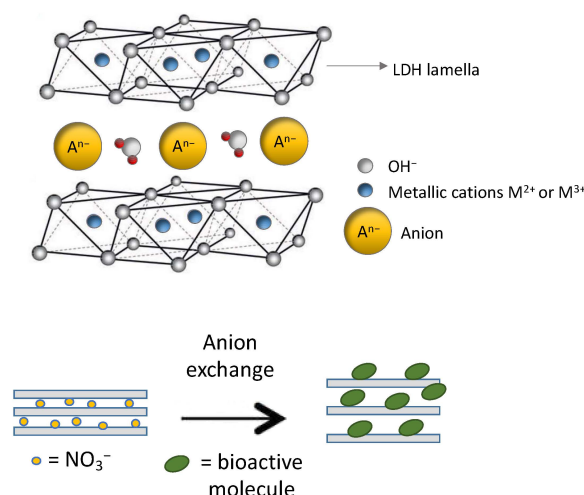


Figure 2. Schematic illustration of the structure of LDH and the anion exchange process of bioactive molecules with nitrate anions.

2. Materials and Methods

2.1. Materials

The magnesium–aluminum layered double hydroxide intercalated with nitrate anion (LDH-NO₃) with the molecular formula [Mg_{0.66}Al_{0.34}(OH)₂](NO₃)_{0.34}·0.5 H₂O was purchased from Prolabin&Tefarm (Perugia, Italy). Trans-ferulic acid (FA-H) 99%, rosmarinic acid (RA-H) 96%, 18β-glycyrrhetic acid (GA-H) 97%, 2,2-diphenyl-1-picrylhydrazyl hydrate (DPPH), 6-hydroxy-2,5,7,8-tetramethylchroman-2-carboxylic acid (Trolox) 97%, linoleic acid ≥ 99%, Tween 20, and β-carotene, all purchased from Sigma-Aldrich (Milan, Italy), were used as received. Table S1 in the Supplementary Materials provides additional data on the purity and properties of commercial FA-H, RA-H, and GA-H. Figure S1 displays the FT-IR spectra of these compounds. IR-grade KBr (Pike Technologies, Fitchburg, WI, USA) was used as received. Ethanol ACS reagent 96% from Sigma-Aldrich (Milan, Italy), acetone ACS reagent ≥ 99.6% and methanol 99+% extra pure from Acros Organics (Geel, Belgium) were used as received. All suspensions were prepared with deionized ultrapure water (18.2 MΩ·cm) obtained using a Milli-Q system (Millipore, Bedford, MA, USA). Table 1 lists the abbreviations of materials used and produced.

Table 1. List of abbreviations.

Abbreviation	Description
FA-H	Trans-ferulic acid
RA-H	Rosmarinic acid
GA-H	18β-glycyrrhetic acid
XA-H	Generic formula for one of the above listed acids
FA	Carboxylate anion of trans-ferulic acid
RA	Carboxylate anion of rosmarinic acid
GA	Carboxylate anion of 18β-glycyrrhetic acid
XA	Generic formula for one of the above listed carboxylate anions
LDH-NO ₃	Mg-Al layered double hydroxide intercalated with nitrate anions
LDH-FA	LDH modified with FA
LDH-RA	LDH modified with RA
LDH-GA	LDH modified with GA
Centrifugate-FA	Supernatant collected after FA immobilization in LDH
Centrifugate-RA	Supernatant collected after RA immobilization in LDH
Centrifugate-GA	Supernatant collected after GA immobilization in LDH
DPPH	2,2-diphenyl-1-picrylhydrazyl hydrate
Trolox	6-hydroxy-2,5,7,8-tetramethylchroman-2-carboxylic acid

2.2. Preparation of Modified LDHs by the Multistage Process

2.2.1. LDH-FA

In the first step of the process, 2 g of LDH-NO₃ was added to 100 mL of CO₂-free water containing 1.47 g (7.57 mmol) of FA-H, equivalent to one times the anion exchange capacity (AEC) of LDH-NO₃ (3.80 meq/g). Subsequently, 398 µL of 50% *w/w* NaOH solution was introduced into the suspension under a nitrogen flow, resulting in a final pH of approximately 8.5. The suspension was stirred for 24 h at room temperature, followed by centrifugation (5000 rpm, 10 min) and washing with deionized water to obtain the LDH-FA_1.1 product. The product was then vacuum dried at 40 °C for 24 h until it reached a constant weight of 2.44 g (Table 2). The supernatant obtained from the centrifugation process (centrifugate-FA_1.1) was analyzed by UV-Vis spectroscopy, revealing the presence of 0.39 g of unreacted ferulate anion (FA) (Table 2). Subsequently, 0.66 g of LDH-NO₃ was added to the deaerated supernatant (by bubbling nitrogen gas for 1 h), and the suspension was stirred for 24 h at room temperature (the pH of the suspension was approximately 8.5). The resulting LDH-FA_1.2 product was obtained through centrifugation, followed by washing with deionized water, and then vacuum dried at 40 °C for 24 h until reaching a constant weight of 0.82 g. The supernatant obtained from this centrifugation step (centrifugate-FA_1.2) contained 0.042 g of FA in 84 mL of solution.

Table 2. Multistage process for the preparation of LDH-FA: yield of the hybrid product, content of FA both in the hybrid products and in the centrifugates.

Step	LDH-FA ¹ (g)	FA in LDH-FA ² (wt.%)	Centrifugate (mL)	FA in the Centrifugate ³ (mg/mL)
1	2.44	37	89	4.3
2	0.82	34	84	0.5

¹ A small amount of product was unintentionally removed during washing. ² The amount of FA in LDH-FA samples was assessed by dissolving 5 mg of each hybrid in 25 mL of 1 M HCl. The absorbance was measured at 323 nm, and the concentration was determined using the calibration curve of FA-H. The percentage was then calculated relative to the total hybrid amount. ³ The FA concentration in each centrifugate was determined by measuring the absorbance at 311 nm and using the calibration curve of NaFA. Both calibration curves were prepared as described in Section 2.3.

2.2.2. LDH-RA

First cycle: An amount of 2 g of LDH-NO₃ was introduced into a 100 mL CO₂-free water solution containing 2.74 g (7.60 mmol) of RA-H, corresponding to one times the AEC of LDH-NO₃. Additionally, 10 mL of EtOH was added to facilitate the solubilization of RA-H. The suspension was stirred under a nitrogen atmosphere for 48 h at room temperature. The pH of the suspension was 5.5–6. The resulting product (LDH-RA_1.1) was obtained through centrifugation and subsequent washing with deionized water. Finally, the product was vacuum dried at 40 °C for 24 h until reaching a constant weight of 2.48 g (Table 3). The supernatant obtained from the centrifugation process (centrifugate_RA_1.1), approximately 90 mL, contained 1.1 g of the rosmarinate anion (RA) (as determined by UV-Vis analysis). Accordingly, 0.72 g of LDH-NO₃ was added to the deaerated supernatant (by bubbling nitrogen gas for 1 h), and the suspension was stirred for 48 h at room temperature. The pH of the suspension was 6–7. The resulting product LDH-RA_1.2 was recovered through centrifugation and washed with deionized water. Finally, the product was vacuum dried at 40 °C for 24 h until a constant weight was achieved (Table 3). The supernatant obtained from the last centrifugation step (centrifugate-RA_1.2) was collected and analyzed.

Second cycle: An amount of 1.37 g (3.80 mmol) of RA-H, equivalent to one times the AEC of LDH-NO₃, was dissolved in a mixture of 50 mL of CO₂-free water and 5 mL of EtOH. Under a nitrogen atmosphere, 1 g of LDH-NO₃ was added, and the suspension was left stirring for 48 h at room temperature. The pH of the suspension was 5.5–6. The resulting product (LDH-RA_2.1) was recovered through centrifugation and washed with deionized water. And vacuum dried at 40 °C for 24 h until a constant weight of 1.55 g (Table 3). The

supernatant obtained after centrifugation (centrifugate-RA_2.1), approximately 34 mL, was collected and immediately acidified using 1 M HCl until a pH of about 3 was reached. The supernatant was analyzed using UV–Vis spectroscopy to determine the amount of unreacted RA (0.28 g), followed by deaeration. Later, 0.2 g of LDH-NO₃ was added and the suspension, covered with an aluminum foil to prevent light interaction, was left stirring for 48 h at room temperature. The resulting product (LDH-RA_2.2) was obtained through centrifugation, washed with deionized water, and vacuum dried at 40 °C for 24 h until a constant weight of 0.30 g was achieved (Table 3). The supernatant obtained from this centrifugation step (centrifugate-RA_2.2) was collected and analyzed.

Table 3. Multistage process for the preparation of LDH-RA: yield of the hybrid product, content of RA both in the hybrid products and in the centrifugates.

Step	LDH-RA ¹ (g)	RA in LDH-RA ² (wt.%)	Centrifugate (mL)	RA in the Centrifugate ³ (mg/mL)
1st cycle				
1	2.48 (2.5)	46	90	12
2	0.94	<3	71	n.d. ⁴
2nd cycle				
1	1.65	48	35	8
2	0.34	43	30	4

¹ A small amount of product was unintentionally removed during washing. ² The amount of RA in LDH-RA samples was assessed by dissolving 5 mg of each hybrid in 25 mL of 1 M HCl. The absorbance was measured at 333 nm, and the concentration was determined using the calibration curve of RA-H. The percentage was then calculated with respect to the total hybrid amount. ³ The RA concentration in each centrifugate was determined by measuring the absorbance at 330 nm and using the calibration curve of RA-H. The calibration curve was prepared as described in Section 2.3. ⁴ Not determined.

2.2.3. LDH-GA

Sodium glycyrrhetinate (NaGA) was synthesized following the method proposed by Wu et al. [33]. In a 50 mL solution containing a 4/1 (*v/v*) mixture of CH₃OH/H₂O, 3 g of GA-H (6.37 mmol) and 335 µL of 50% *w/w* NaOH solution were dissolved. The reaction mixture was stirred for 1 h, followed by partial solvent evaporation. Next, 15 mL of ethyl acetate was added, and the resulting residue was cooled to −20 °C for 24 h. The precipitation of NaGA was repeated by adding another 15 mL of ethyl acetate and cooling. The solid was filtered, washed with acetone, and dried, producing 2.5 g of NaGA as a white solid.

In the first step of the process, 1 g of LDH-NO₃ was added to 50 mL of CO₂-free water/EtOH 60/40 *v/v* solution containing 1.87 g (3.80 mmol) of NaGA, equivalent to one times the AEC of LDH-NO₃. The suspension was stirred for 24 h at room temperature, followed by centrifugation (5000 rpm, 10 min) and washing with deionized water to obtain the LDH-GA_1.1 product. The product was then vacuum dried at 40 °C for 24 h until it reached a constant weight of 1.1 g (Table 4).

The supernatant obtained from the centrifugation process (centrifugate-GA_1.1) was analyzed by UV–Vis spectroscopy, revealing the presence of 1.33 g of unreacted GA (Table 4). Subsequently, 0.75 g of LDH-NO₃ was added to the deaerated supernatant, and the suspension was stirred for 24 h at room temperature (the pH of the suspension was approximately 7–8). The resulting LDH-GA_1.2 product was obtained through centrifugation, followed by washing with deionized water, and then vacuum dried at 40 °C for 24 h until reaching a constant weight of 0.8 g. The supernatant obtained from this centrifugation step (centrifugate-GA_1.2) contained 1.07 g of GA in 37 mL of solution.

Table 4. Multistage process for the preparation of LDH-GA: yield of the hybrid product, content of FA both in the hybrid products and in the centrifugates.

Step	LDH-GA ¹ (g)	GA in LDH-GA ² (wt.%)	Centrifugate (mL)	GA in the Centrifugate ³ (mg/mL)
1	1.1	12	43	31
2	0.8	10	37	29

¹ A small amount of product was unintentionally removed during washing. ² The amount of GA in LDH-GA samples was assessed by dissolving 2–3 mg of each hybrid in a few drops of concentrated HCl and then diluting it in EtOH. The absorbance was measured at 250 nm, and the concentration was determined using the calibration curve of GA-H. The percentage was then calculated relative to the total hybrid amount. ³ The GA concentration in each centrifugate was determined by measuring the absorbance at 250 nm and using the calibration curve of NaGA. Both calibration curves were prepared as described in Section 2.3.

2.3. Characterization

A full description of the instruments and methods of characterization is given in the Supplementary Materials.

2.4. Antioxidant Activity

2.4.1. DPPH Assay

A description of the DPPH assay is reported in the Supplementary Materials.

2.4.2. β -Carotene/Linoleic Acid Assay

A stock solution of β -carotene and linoleic acid was prepared using the following procedure: 0.5 mg of β -carotene was dissolved in 1 mL of CHCl_3 , and 25 μL of linoleic acid, along with 200 mg of Tween 20, were added. The CHCl_3 was then completely vacuum evaporated. Subsequently, with vigorous shaking, 100 mL of distilled water saturated with oxygen (30 min at 100 mL/min) was added. A volume of 2.5 mL of this reaction mixture was transferred into a cuvette, and 350 μL of pure antioxidant methanol solutions (concentration of 2 mg/mL) or methanol LDH suspensions (the antioxidant concentration in each LDH suspension is 2 mg/mL) was added to create an emulsion. The incubation of the emulsion took place at 40 °C. Readings of all samples at 460 nm were performed immediately ($t = 0$ min) and after 180 min of incubation. After 180 min the decrease in the absorbance of the control sample was no longer significant. The control sample was prepared in the same way as the reacting mixture but adding only 350 μL of MeOH. In addition, an emulsion without β -carotene mixed with 350 mL of MeOH was used for the baseline. The same procedure was repeated using Trolox as a positive control. The antioxidant activity (AOA) was expressed using the following equation [34,35]:

$$AOA = \left[\frac{(A_{a,180} - A_{b,180})}{(A_{b,0} - A_{b,180})} \right] \times 100 \quad (1)$$

where $A_{a,180}$ is the absorbance of the sample at 180 min and $A_{b,180}$ and $A_{b,0}$ are the absorbances of the control sample at 180 and 0 min, respectively.

3. Results and Discussion

This study describes a multistage method for immobilizing the carboxylate anions of FA-H, RA-H, and GA-H (referred to as XA-H) onto LDH- NO_3 through anion exchange (Figure 3). Initially, LDH-XA_1.1 was formed and recovered through centrifugation, while the remaining solution, called centrifugate-XA_1.1, was UV-Vis analyzed in order to determine the concentration of residual carboxylate anions. In the subsequent synthesis step, an amount of LDH- NO_3 , equimolar to residual carboxylate anions, was added to centrifugate-XA_1.1, initiating the second step of the anion exchange. The resulting product, LDH-XA_1.2, was recovered through centrifugation, yielding a second centrifugate named centrifugate-XA_1.2. The concentration of residual organic anions in this latter centrifugate

was measured, and based on the determined value, a decision was made on whether to proceed with additional anion exchange steps or not.

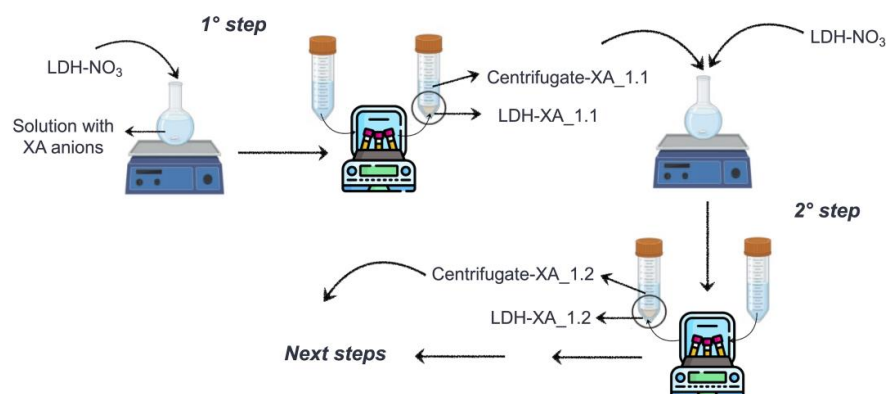


Figure 3. Diagram of the multistage process used to immobilize carboxylate anions into LDH-NO₃.

The distinctive feature of this methodology resides in its capacity to continuously monitor and regulate the residual concentration of organic anions at each synthesis step, thus facilitating tailored adjustments in order to meet specific requirements.

During all synthesis steps, the LDH-XA obtained from the anion exchange and the corresponding centrifugate underwent characterization by the aim of FT-IR and UV-Vis spectroscopic analyses. Additionally, LDH-XA underwent XRD analysis, confirming the insertion of the organic anions in between the layers or their adsorption on the surface of the layers.

3.1. Immobilization of FA-H

To prepare LDH-FA, we followed the previously outlined method, and, from the first step, we obtained the hybrid product LDH-FA_1.1 and the centrifugate-FA_1.1. Then, we measured the concentration of FA in the centrifugate by UV-Vis analysis and, based on the results, we conducted a second step of anion exchange to obtain LDH-FA_1.2 and centrifugate-FA_1.2.

By FT-IR spectroscopy, we verified the presence of the ferulate anions in both LDH-FA hybrids through meaningful comparisons with the spectra of FA-H and NaFA (Figure 4a). The FA-H spectrum showed the characteristic band of carboxyl stretching vibrations $\nu(\text{C}=\text{O})$ at $1692\text{--}1668\text{ cm}^{-1}$, the stretching vibration of the alkene double bond, $\nu(\text{C}=\text{C})$, at 1620 cm^{-1} , and a band at 3437 cm^{-1} attributed to the stretching vibration of the OH substituent in the aromatic ring, $\nu(\text{OH})_{\text{ar}}$ [36]. Notably, this band shifted to 3413 cm^{-1} in the NaFA spectrum due to the coordination of the OH groups with sodium cations resulting in a decrease in the electron charge density of the O-H bond compared to the acidic species [36]. The FT-IR spectrum of NaFA also disclosed the vibration of the aromatic ring at 1598 cm^{-1} , stretching vibrations of the carboxylate group at 1517 cm^{-1} $\nu(\text{COO})_{\text{as}}$ and at 1388 cm^{-1} $\nu(\text{COO})_{\text{s}}$ [37], along with bands at 1126 and 1032 cm^{-1} assignable to the C-O stretching mode of the phenolic and methoxy groups, respectively.

The FT-IR spectra of LDH-FA_1.1 and LDH-FA_1.2 showed typically LDH bands due to the OH stretching vibration at approximately 3450 cm^{-1} , which was broadened compared to that observed for LDH-NO₃, most likely due to host-anion interactions, and the Mt-O vibrational modes such as those at 447 cm^{-1} and 680 cm^{-1} (Figure 4a). Both spectra showed a decrease/disappearance in the nitrate anion band (1380 cm^{-1}) and the appearance of bands corresponding to asymmetric and symmetric stretching vibrations of the carboxylate group at $1518\text{--}1519\text{ cm}^{-1}$ and $1399\text{--}1400\text{ cm}^{-1}$, respectively, along with the C=C stretching at 1634 cm^{-1} . Notably, the carboxylate asymmetric stretching bands of the two samples exhibited distinct shoulders at 1542 and 1541 cm^{-1} , respectively, suggesting the potential presence of multiple coordination modes of carboxylate groups at the lamellae (Figure S2).

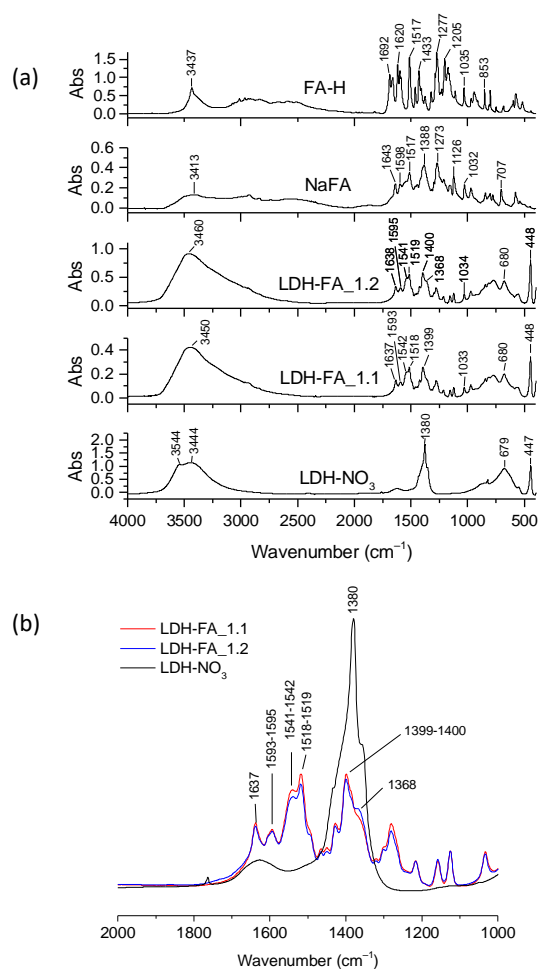


Figure 4. Representative FT-IR spectra of LDH-NO₃, LDH-FA_1.1, LDH-FA_1.2, NaFA, and FA-H (a). Enlarged view of the spectra of LDH-NO₃, LDH-FA_1.1, and LDH-FA_1.2 in the absorption range between 2000 and 1000 cm⁻¹. The spectra have been normalized to the LDH absorption band at 447 cm⁻¹ (b).

It is known that carboxylate groups can coordinate in various ways with metal-containing species, such as LDH, causing fluctuations in the frequency difference between asymmetric and symmetric stretching modes ($\Delta\nu = \nu_{as} - \nu_s$) [38,39]. Previous studies have demonstrated that free carboxylate anions, typically those of the sodium or potassium salts, and carboxylate groups in bridging bidentate coordination give similar $\Delta\nu$ values. In contrast, the bidentate chelating coordination reduces the frequency difference [39]. Moreover, these previous studies suggested that symmetrical bridging or chelation mode shifts both frequencies in the same direction. In our case, we found that the $\Delta\nu$ values of LDH-FA_1.1 and LDH-FA_1.2 (Table S2) were slightly lower compared to the NaFA $\Delta\nu$ value. This result suggests that carboxylate groups might bind to the metallic ions in the LDH layers through a chelate-bidentate or bridged-bidentate mode, favoring different geometries in the arrangement of the ferulate species in the interlayer space. The observed frequency variations in the carboxylate group stretching may also be attributed to the presence of different types of cations in the layers, such as Mg and Al.

To compare the quantity of ferulate anions immobilized on LDH-FA_1.1 and LDH-FA_1.2, we normalized their FT-IR spectra to the Mg-O vibration of the layers at 447 cm⁻¹ (Figure 4b). Both spectra showed FA carboxylate anion bands of similar intensity. Therefore, we quantified the amount of FA in the LDH products and centrifugates using UV-Vis spectroscopy with appropriate calibration curves (see description in Materials and Methods). The analysis revealed that 37 wt.% of LDH-FA_1.1 comprises the ferulate anion, while

the centrifugate-FA_1.1 had a ferulate anion equivalent to 25 wt.% of initial FA-H. In the second anion exchange step, the LDH-FA_1.2 product was produced with a 35 wt.% FA composition. It is noteworthy that the second step was equally effective in immobilizing the organic anion as the first step. Lastly, the centrifugate resulting from the second step had only 1.3% of the initial content of FA-H. Hence, the synthesis process concluded without further steps.

The XRD diffractograms of LDH-FA_1.1 and LDH-FA_1.2 samples (Figure 5) revealed a diffraction signal (003) at lower angles (with a maximum at 5.1°) compared to their precursor LDH-NO₃ (9.9°), indicating the intercalation of the anion between the lamellae [14,40]. Additionally, both LDH_FA_1.1 and LDH_FA_1.2 exhibited a signal at approximately 10.5° attributed to the (006) reflection of the intercalated product, with less intense signals observed at higher angles, likely corresponding to higher order reflections. In the case of LDH_FA_1.1, and more prominently in LDH_FA_1.2, the (003) reflection comprises two overlapping signals with maxima at 5.1 and 3.9° , corresponding to a d-value of 1.7 and 2.3 nm, respectively. By considering the dimensions of the ferulate anion obtained by semi-empirical calculations ($1.8 \times 7.1 \times 9.4 \text{ \AA}$), possibly the ferulate can arrange in the interlamellar space as both a monolayer and a bilayer [16,40,41]. The basal distance corresponding to the monolayer arrangement aligns with the 5.1° signal while the bilayer arrangement leads to an increase in the interlamellar space consistent with the 3.9° signal.

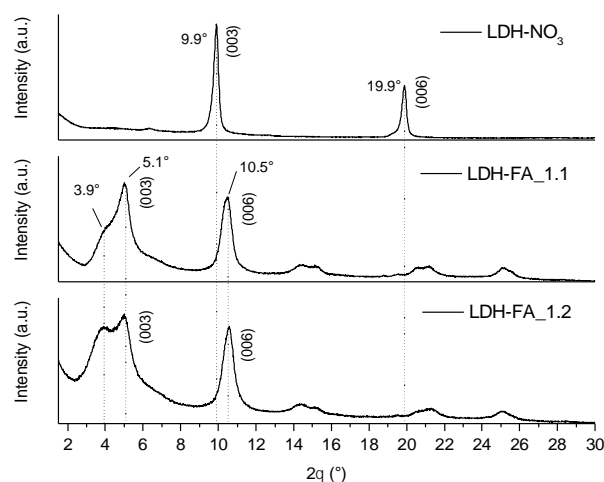


Figure 5. XRD patterns of LDH-NO₃, LDH-FA_1.1, and LDH-FA_1.2 in the 2θ interval $1.5\text{--}30^\circ$.

The TGA analysis of LDH-FA_1.1 and LDH-FA_1.2 confirmed the uniformity of the two samples. They showed similar thermograms with comparable residue values of approximately 39 wt.% (Figure 6).

The thermograms of LDH-FA_1.1, and LDH-FA_1.2 showed a first weight loss at a maximum temperature of 93°C which can be attributed to the water loss. Interestingly, this weight loss occurred at a lower temperature than in the LDH-NO₃ sample, indicating that FA reduced the interaction between water molecules and OH groups within the lamellae. A second weight loss occurred between 150 and 250°C , and it was due to the desorption and initial decomposition of ferulate anions, likely those adsorbed on the lamellae that are more susceptible to heat. A comparison with the NaFA thermogram (Figure S3) suggests that FA degradation occurs within this temperature range. Due to the FA's decarboxylation, 4-vinyl guaiacol and guaiacol can potentially be produced as primary products during this degradation step [42]. The third stage of weight loss for LDH-FA occurred between 250 and 600°C , causing complete degradation of the organic anion adsorbed and intercalated between the LDH lamellae. The degradation of the organic anion occurred at this stage simultaneously with the dehydroxylation of the lamellae. This analysis confirms that LDH-FA_1.1 and LDH-FA_1.2 have similar compositions, but it also highlights that the two products are thermally unstable at temperatures exceeding 150°C .

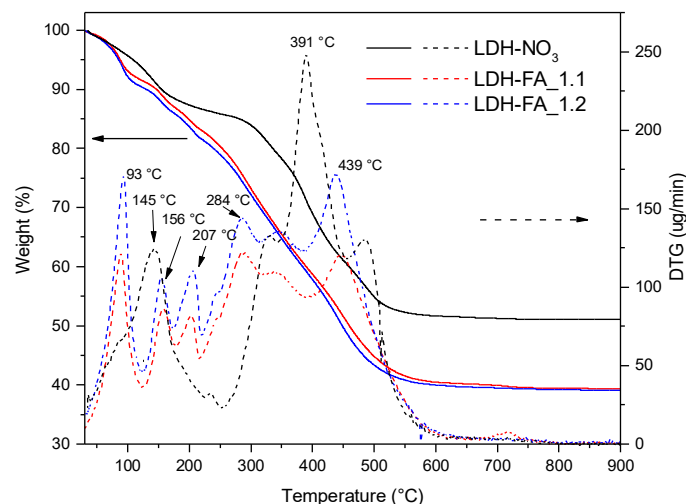


Figure 6. TG/DTG thermograms of LDH-NO₃, LDH-FA_1.1, and LDH-FA_1.2.

3.2. Immobilization of RA-H

The process of RA-H immobilization in LDH-NO₃ was carried out without the addition of a base, as the aqueous suspension of LDH-NO₃ and RA-H has a pH of about 5 allowing the formation of the carboxylate anion (RA-H pKa₁ is 2.9) without generation of the phenate anion [43].

The first step of the process yielded the LDH-RA_1.1 product, incorporating the RA anion, as confirmed by the FT-IR spectrum, which shows an absorption band at 1587 cm⁻¹ attributed to the asymmetric stretching of the carboxylate group ($\nu_{as}(\text{COO})$), in agreement with the spectrum of the sodium salt NaRA (Figure S4). Subsequent UV-Vis analysis revealed that LDH-RA_1.1 contained 46 wt.% of RA. In the second step, LDH-NO₃ was introduced to the centrifugate-RA_1.1 derived from the first step, aiming at recovering the non-immobilized RA anions. However, the resulting LDH-RA_1.2 sample exhibited minimal RA immobilization as evidenced by the FT-IR spectrum. Indeed, the predominant presence of the IR absorption band at 1381 cm⁻¹ was associated to the stretching mode of the non-exchanged nitrate anions, and the weak absorption band at 1587 cm⁻¹ was attributed to the RA anion (Figure S4). In addition, UV-Vis analysis of the LDH-RA_1.2 product confirmed that the RA content was less than 3 wt.%.

To delve deeper into this finding, we isolated and analyzed the centrifugate over time. We observed a rapid darkening and the formation of a precipitate, which was soluble in water but insoluble in organic solvents such as methanol, acetone, chloroform, and dichloromethane (Figure S5). The UV-Vis spectrum of centrifugate-RA_1.1 revealed a band at approximately 330 nm, attributed to the double bond conjugated to the aromatic ring of RA-H (Figure S6a). This band diminished in intensity over time, accompanied by the emergence of a broad, low-intensity band at approximately 420 nm which emerged when comparing the UV-Vis spectrum of the solution stored for seven days with the freshly obtained centrifugate, as illustrated in Figure S6b.

The behavior of the centrifugate is likely due to the possible autoxidation of RA-H in analogy with other catechols. Polyphenolic compounds, in contact with oxygen, are responsible for the browning of fruits and vegetables, leading to colored macromolecular structures and unpleasant flavor formation. This process occurs by autoxidation or is catalyzed by enzymes and is faster under alkaline reaction conditions [44]. The exact mechanisms behind these processes still need to be fully understood. A general reaction sequence is the oxidation of *o*-diphenol in the catechol group, followed by the formation of a semiquinone that can condense into various structures [44]. For instance, in the case of caffeic acid, which is another type of catechol, it has been observed that the reduction in the intensity of the UV band at 330 nm is related to the involvement of the double bond in the formation of dimers, trimers, and oligomers [45]. Caffeic acid and catechols probably follow

oxidative polymerization mechanisms that involve different groups (Figure S7), leading to the formation of substituted tetrahydrofuran structures, to molecules like the 2,3-dihydro-1,4-benzodioxin called caffeicin, and ring condensation via an ether formation or a direct C-C bond formation between two free positions in the benzene rings [46]. Interestingly, molecules with structures like that reported in Figure S7 were detected in the extract of *Celastrus hindsii* together with RA-H, suggesting that RA-H can give dimers and trimers like caffeic acid [47]. These compounds can be responsible for the dark stain and the appearance of the band at 420–430 nm. The alteration in the color of centrifugate-RA_1.1 and the presence of the 420 nm band in the UV spectrum suggested the existence of oxidized RA species within the centrifugate. This centrifugate was stored without specific precautions before the initiation of the second step and had a pH of approximately 6–7.

Therefore, we replicated the modification experiment collecting the product LDH-RA_2.1 from the first step by taking necessary precautions to prevent any possible oxidation of the centrifugate-RA_2.1. We quickly acidified the centrifugate-RA_2.1, which was stored in an inert atmosphere and under light exclusion until the next interaction with LDH-NO₃. The UV-Vis spectrum of the centrifugate remained unchanged over time, as well as its color. Therefore, the acidic pH, the absence of light, and the inert atmosphere prevented RA from oxidation. As a result of this second experiment, we obtained samples LDH-RA_2.1 and LDH-RA_2.2.

The FT-IR spectra of LDH-RA_2.1 and LDH-RA_2.2 products showed characteristic absorptions indicative of RA compared to those of LDH-NO₃, RA-H, and NaRA (Figure 7a). Furthermore, normalizing these spectra and that of LDH-NO₃ relative to the reference absorption band at 447 cm⁻¹, we observed that the relative height of the characteristic RA absorption bands is comparable in both products, albeit more pronounced in the LDH-RA_2.1 sample (Figure 7b). According to UV-Vis analysis, the amount of RA immobilized on LDH-RA_2.1 was 48 wt.%, similar to the result found in the first experiment for the LDH-RA_1.1 sample. For the LDH-RA_2.2 sample obtained in the second step of the second experiment, the RA amount was 43 wt.%. These results show that our strategy to preserve the centrifugate before the next anion exchange step effectively prevents RA's oxidation into oligomers, enabling the recovery of the anion in a subsequent immobilization phase on fresh LDH-NO₃. Additionally, the centrifugate-RA_2.2 retained about 9% of the initial RA-H content, which can be recovered through an additional immobilization step.

Comparing the diffractograms of the LDH-RA products (Figure 8) obtained in various tests, it is evident that LDH-RA_1.1 displays diffraction signals at 3.8° and 7.4°, which can be attributed to the (003) and (006) reflections of the intercalated product. Interestingly, LDH-RA_1.2, resulting from the second step of the first test, exhibits the (003) and (006) reflections of LDH-NO₃, confirming that the intercalation of RA was not feasible under these conditions. In the other hybrids, in addition to the diffraction signals at 3.8° and 7.4°, reflections at 9.9° and 19.9° are still observable (particularly for LDH-RA_2.2), which indicated that a small fraction of LDH-NO₃ did not participate in the RA exchange process.

The TGA analysis conducted on the LDH-RA hybrid systems from the first trial (Figure 9) showed that the two samples had different residue values (27 wt.% for LDH-RA_1.1 and 49 wt.% for LDH-RA_1.2). This difference was due to a variation in the organic fraction content, in agreement with previously discussed findings. The TGA curve of the LDH-RA_1.1 sample revealed an initial weight loss between 30 and 200 °C, attributable to the removal of adsorbed and intercalated water between the layers. Then, a further weight loss between 200 and 250 °C corresponds to the desorption and initial decomposition of the RA anions immobilized in the layered system. This is similar to the TGA curve obtained for pure RA-H and NaRA, as shown in Figure S8. Finally, a last stage was observed in the range of 250–600 °C, attributed to the complete degradation of RA anions and dehydroxylation of the layers. This temperature range also includes the decomposition of any nitrate anions, as highlighted in the TGA curve of LDH-NO₃ (Figure 6). The decomposition of nitrate anions was visible in the thermogram of LDH-RA_1.2, confirming that the RA exchange, in this case, was unsuccessful. On the other hand, comparing the thermograms of the

LDH-RA products obtained from the second trial (LDH-RA_2.1 and LDH-RA_2.2), it was confirmed that by maintaining the centrifugate under suitable conditions of acidification and protection from oxidation, it is possible to obtain the LDH-RA_2.2 product, with an organic/inorganic hybrid composition comparable to the LDH-RA_2.1 product (Figure 9).

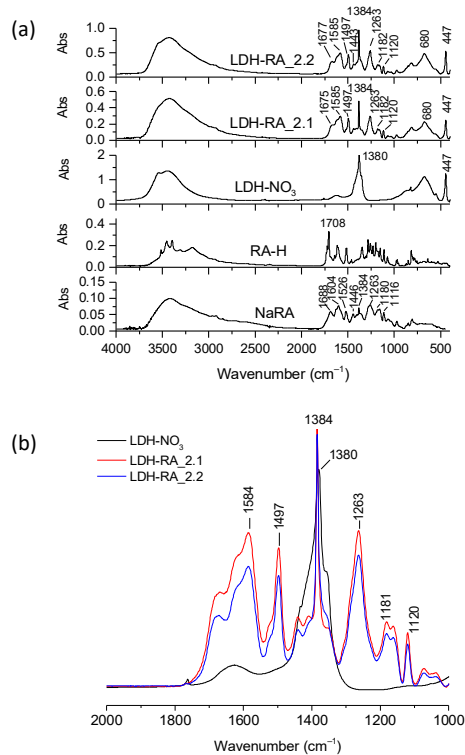


Figure 7. Representative FT-IR spectra of LDH-NO₃, LDH-RA_2.1, LDH-RA_2.2, NaRA, and RA-H (a). Enlarged view of the spectra of LDH-NO₃, LDH-RA_2.1, and LDH-FA_2.2 in the absorption range between 2000 and 1000 cm⁻¹. The spectra have been normalized to the LDH absorption band at 447 cm⁻¹ (b).

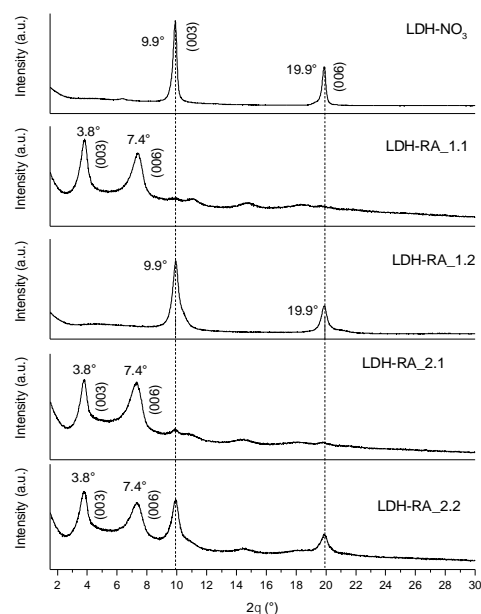


Figure 8. XRD patterns of LDH-NO₃, LDH-RA_1.1, LDH-RA_1.2, LDH-RA_2.1, and LDH-RA_2.2 in the 2θ interval 1.5–30°.

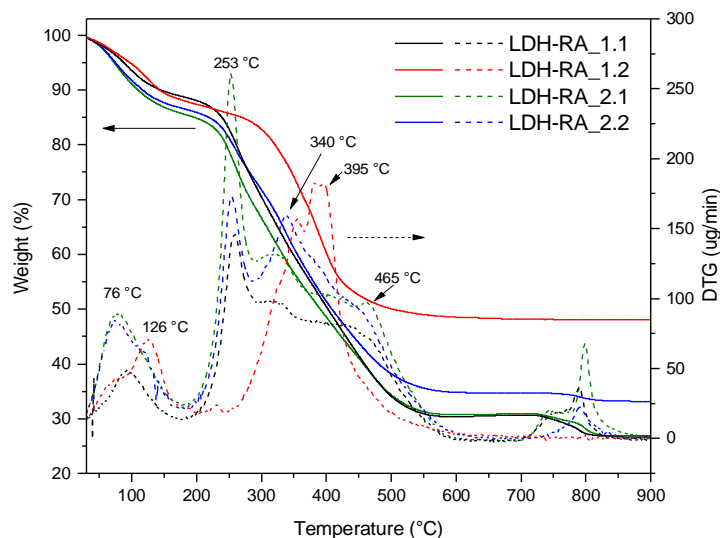


Figure 9. TG/DTG thermograms of LDH-RA_1.1, LDH-RA_1.2, LDH-RA_2.1, and LDH-RA_2.2.

3.3. Immobilization of GA-H

The initial step of the anion exchange process yielded the LDH-GA_1.1 product and the centrifugate-GA_1.1. The subsequent step resulted in forming the solid product LDH-GA_1.2 and the centrifugate-GA_1.2.

The FT-IR spectra of the LDH-GA samples were compared with those of GA-H and NaGA to confirm that the GA anion was incorporated (Figure 10a). Although the stretching bands of the ketone group at 1644 cm^{-1} ($\nu(\text{C}=\text{O})$) and the asymmetric vibration mode of the carboxylate anion at 1540 cm^{-1} ($\nu_{\text{as}}(\text{COO}^-)$) were visible. Their intensity was relatively low. Notably, the GA bands were more visible in LDH-GA_1.1 than in LDH-GA_1.2, as shown in Figure 10b. Additionally, spectra of the hybrids showed an absorption at 1380 cm^{-1} with a shoulder at 1360 cm^{-1} . The signal at 1380 cm^{-1} was due to the stretching of the nitrate anions, which were not involved in the anion exchange process. The shoulder at 1360 cm^{-1} was likely due to the stretching of carbonate anions that became part of the structure of the modified products during the modification or washing phase.

These results suggest that the anion exchange was unsuccessful, as evidenced by the high concentration of anions in the centrifugates (Table 4). UV-Vis analysis showed that LDH-GA_1.1 contained 12 wt.% of GA immobilized on the LDH, with approximately 75% of the GA initially introduced into the reaction vessel found in the centrifugate-GA_1.1. Similarly, LDH-GA_1.2 contained 10 wt.% of GA, and the centrifugate-GA_1.2 included 60% of the initial GA quantity.

XRD patterns of the two LDH-GA products (Figure S9) did not show any shift in the reflection bands towards lower angles, indicating that GA is not inserted between the LDH layers but is likely adsorbed on the surface. Moreover, the diffraction patterns also revealed a splitting of the (003) diffraction signal, with one peak consistent with the (003) diffraction of LDH-NO₃ and another at approximately 10.4° attributed to the incorporation of carbonate anions into the structure [48], corroborating results obtained by FT-IR analysis.

The SEM micrographs of LDH-FA, LDH-RA, and LDH-GA (Figure S10) further support the hypothesis that in the case of LDH-GA, the anion is solely adsorbed on the external surface of the particles. In the case of LDH-GA, aggregates with a smoother surface are evident, distinguishing them from the two intercalated systems and indicating a surface coating on the particles. This behavior can be attributed to the more significant steric hindrance of GA compared to FA and RA, along with the tendency of GA-H to form self-assembling hydrogels, increasing the overall size of the organic fraction to be intercalated [33]. Since GA is only adsorbed on the surface of LDH-NO₃ particles, the available surface area for anchoring is limited compared to an intercalated system, leading to reduced

retention. Consequently, LDH-GA hybrids exhibited lower GA content than LDH-RA and LDH-FA samples.

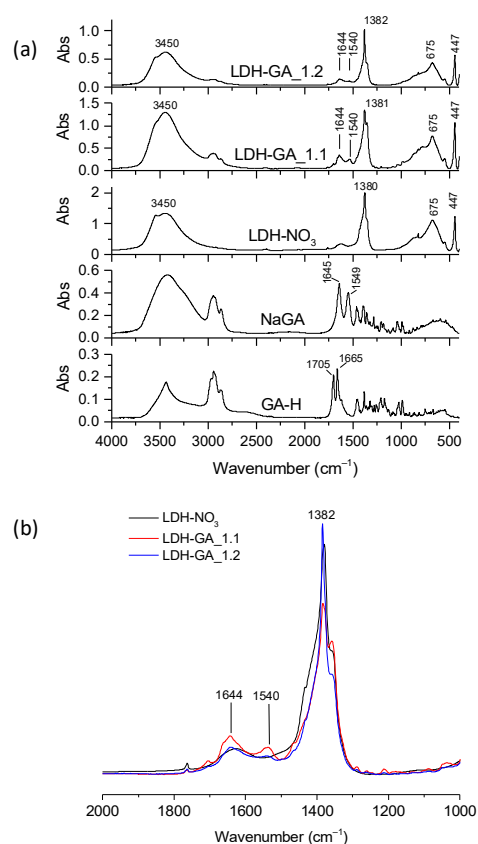


Figure 10. Representative FT-IR spectra of LDH-NO₃, LDH-GA_1.1, LDH-GA_1.2, NaGA, and GA-H (a). Enlarged view of the spectra of LDH-NO₃, LDH-GA_1.1, and LDH-GA_1.2 in the absorption range between 2000 and 1000 cm⁻¹. The spectra have been normalized to the LDH absorption band at 447 cm⁻¹ (b).

The TGA analysis of the two hybrid products confirmed the presence of an organic fraction in quantities consistent with those determined through UV-Vis analysis. The residue was lower than that of LDH-NO₃, measuring 46 wt.% and 48 wt.% for LDH-GA_1.1 and LDH-GA_1.2, respectively (Figure S11). In addition, thermograms revealed a weight loss between 250 and 550 °C, representing a combination of multiple degradation steps, including layer dehydroxylation and thermal decomposition of both inorganic and organic anions, as evidenced by comparison with the NaGA thermogram.

3.4. Antioxidant Capacity of LDH-FA and LDH-RA

Phenolic compounds, such as RA-H and FA-H, are known for their antioxidant activity, protecting against oxidative damage caused by free radicals [49]. Excessive free radicals are implicated in skin aging and various diseases. Furthermore, in food, the lipid oxidation induced by free radicals is a critical factor in storage and processing deterioration. Among biologically relevant free radicals, alkyl peroxy radicals and singlet oxygen require neutralization to delay oxidative destruction.

To assess the antioxidant activity of our phenolic compounds, we evaluated the efficacy of RA-H and FA-H, along with their hybrid products LDH-RA and LDH-FA, in neutralizing DPPH radicals and alkyl peroxy radicals in the β -carotene–linoleic acid emulsion system.

The DPPH test, a standard method for assessing antioxidant potential, measured the decrease in DPPH absorbance, with a color change from purple to yellow, indicating

antioxidant neutralization. The EC₅₀ results revealed that RA-H exhibited significantly higher antioxidant activity than FA-H and Trolox used as reference compound (Table 5).

Table 5. EC₅₀ by DPPH test and antioxidant activity by β -carotene/linoleic acid test of Trolox, FA-H, RA-H, selected LDH-FA, and LDH-RA.

Sample	DPPH Test EC ₅₀ (μ M) ¹	β -Carotene/Linoleic Acid Test Antioxidant Activity (AOA %) ²
Trolox	23 \pm 3	100
FA-H	19 \pm 1	24
RA-H	2.7 \pm 0.1	55
LDH-FA	17 \pm 1 ²	97
LDH-RA	19 \pm 7 ²	97

¹ Mean value of three runs \pm standard deviation. ² These EC₅₀ values were calculated considering the theoretical molar concentration of XA-H available in selected LDH-RA (46 wt.%) and LDH-FA (37 wt.%). ² AOA was calculated as described in Equation (1).

We found that LDH-FA had a similar EC₅₀ value to free FA-H. In contrast, LDH-RA had a higher EC₅₀ value than RA-H, which indicates that the hybrid system has a lower antioxidant capacity than the free molecule. However, considering that the concentration of RA in the methanolic suspension used for the test may be lower than the maximum value determinable from the composition of LDH-RA due to its dependence on the migration kinetics of RA, the obtained EC₅₀ value might not accurately represent the actual value. To this aim, we made a preliminary recalculation of LDH-RA EC₅₀ by determining the concentration of RA in test solutions using absorbance at 311 nm. As a result, the estimated EC₅₀ value for LDH-RA was 1.9 \pm 0.7, closely resembling that obtained for RA-H.

The β -carotene/linoleic acid test measures the bleaching of β -carotene due to oxidation caused by linoleic acid degradation products. This test estimates how well an antioxidant protects lipids in biological systems [35,50]. Antioxidants compete with β -carotene for alkyl peroxy radicals, and this test reveals the antioxidant activity of various substances. The test showed that RA-H and FA-H had a lower antioxidant capacity than Trolox (Table 5). However, RA-H showed a higher antioxidant activity than FA-H, supported by existing literature [49]. Surprisingly, the antioxidant activity of the two hybrid systems was almost as high as that of Trolox. In an initial assessment, the superior performance of the immobilized species could be attributed to the synergy between the structure of the inorganic support and the chemical properties of the phenolic acid, making it a more effective system in combating oxidative processes than free phenolic acid. However, it cannot be excluded that the LDH may have interfered during the test by immobilizing linoleic acid and limiting its oxidation. Further tests will be required to validate these results and determine the exact mechanism.

3.5. UV Shielding Capacity of LDH-RA

It has been shown that derivatives of cinnamic and hydroxycinnamic acids, such as FA-H and RA-H, are effective UV filters [17,18,37]. As a result, they can be used as active components in photoprotective products like sunscreens. FA immobilized in a hydrotalcite is chemically and thermally stable and effectively controls diffusion by limiting release and other associated adverse effects [14]. Additionally, the LDH-FA hybrid system is transparent in the visible range and absorbent in the UV region, making it a potential candidate for use as an optical filter [17]. We then evaluated whether LDH-RA also possesses UV-filtering ability, and to do this test we recorded the reflectance UV-Vis absorption spectrum of LDH-RA_1.1 (Figure 11).

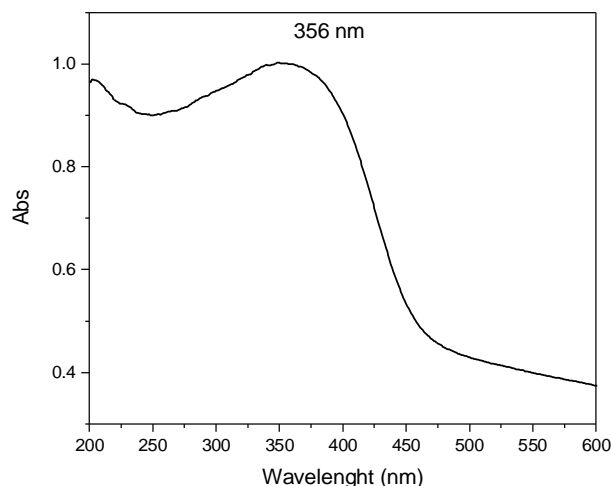


Figure 11. Absorption spectrum of LDH-RA_1.1.

The spectrum showed an absorption band at 356 nm, confirming the presence of RA in the hybrid system. Notably, this band was redshifted compared to the RA-H spectrum in solution (333 nm). This effect was likely due to increased π - π interaction resulting from intermolecular interactions among RA molecules in the solid state. Furthermore, the sample showed absorption in the UV region and partially in the visible spectrum, indicating its potential use as an optical filter.

4. Conclusions

This study aimed at developing modified LDH using natural compounds known for their antioxidant, antimicrobial, and anti-inflammatory properties: FA-H, RA-H, and GA-H.

The LDH modification process involved an anion exchange mechanism whereby the carboxylate anions of the chosen acids replaced the nitrate anions. Furthermore, repeating the process with reaction waters still containing unreacted carboxylate anions allowed for immobilizing most of the active substance on LDH lamellae with limited loss of valuable substance. This approach, in line with sustainable practices, helped enhance the yield of modified LDH by reducing unreacted XA-H and water consumption in all steps.

Detailed analyses (FT-IR, XRD, TGA, and UV-Vis) conducted on the modified LDHs (LDH-RA, LDH-FA, and LDH-GA) provided valuable insights. It was found that residues from the previous step could be directly used to obtain new batches of modified LDH for FA-H and GA-H. However, procedural modifications were necessary for RA-H to prevent the decomposition of the carboxylate anion, involving acidification and storage in an inert and dark environment before another exchange with LDH-NO₃. This procedural modification also proved effective in recovering the unreacted carboxylate anion.

Analyses revealed that the modified LDHs contained an organic fraction ranging from 10% to 48% by weight. XRD data indicated that FA and RA were intercalated between the LDH layers while the GA anion was adsorbed onto the surface.

Further investigations proved that these lamellar hybrid systems could play a significant role in practical applications for cosmetic and dermatological formulations. Indeed, antioxidant capacity measurements confirmed the preservation of the antioxidant activity of free molecules in LDH-RA and LDH-FA suspensions, as demonstrated by the DPPH and β -carotene-linoleic acid assays. Additionally, the antioxidant activity of the two hybrid systems approached that of Trolox, a widely used commercial product. Moreover, UV-Vis analysis confirmed the potential of LDH-RA as a sunscreen.

In summary, this study demonstrated the effectiveness of the LDH modification process using natural compounds, highlighting their potential applications in cosmetics. It also emphasized the importance of sustainable considerations in designing synthesis procedures to make them more efficient, socially acceptable, and environmentally friendly.

Furthermore, the method developed here offers the potential for the direct treatment of agri-food residue extracts, providing significant benefits to the agri-food industry through applying circular economy principles.

Supplementary Materials: The following supporting information can be downloaded at: <https://www.mdpi.com/article/10.3390/cosmetics11020052/s1>, Table S1: Physicochemical data of commercial FA-H, RA-H, and GA-H. Figure S1: FT-IR spectra of commercial FA-H, RA-H, and GA-H. Characterizations: DPPH assay. Figure S2: FT-IR spectra in the region 1800–1000 cm^{-1} of (a) LDH- NO_3 , (b) LDH-FA_1.1, (c) LDH-FA_1.2, and (d) NaFA. Table S2: Frequencies of the carboxylate asymmetric and symmetric stretching modes and frequency difference values ($\Delta\nu = \nu_{\text{as}} - \nu_{\text{s}}$) between carboxylate stretching modes of NaFA and LDH-FA samples. Figure S3: TG/DTG thermogram of NaFA. Figure S4: Representative FT-IR spectra of LDH- NO_3 , LDH-RA_1.1, LDH-RA_1.2, and NaRA. Figure S5: Images of the centrifugate-RA_1.1 acquired over 7 days (unprotected storage). Figure S6: UV-Vis spectra of centrifugate-RA_1.1 at time zero and after seven days of storage in a non-inert atmosphere; difference between the two spectra (b). Figure S7: Possible autoxidation mechanisms of RA-H and derived products; other isomers are possible. *Position of bond with the other carboxylic group of RA; Figure S8: TG/DTG thermograms of RA-H and NaRA. Figure S9: XRD patterns of LDH- NO_3 , LDH-GA_1.1, and LDH-GA_1.2 in the 2θ interval 1.5–30°. Figure S10: Representative SEM micrographs of LDH-FA (a), LDH-RA (b), and LDH-GA (c). Figure S11: TG/DTG thermograms of LDH-GA_1.1, LDH-GA_1.2, LDH- NO_3 , and NaGA.

Author Contributions: Conceptualization, S.C., E.P. and F.C.; methodology, S.C., E.P., M.-B.C. and F.C.; validation, S.C., E.P., A.T., W.O., M.-B.C. and F.C.; formal analysis, S.C.; investigation, S.C., E.P., A.T., W.O., M.-B.C. and F.C.; resources, E.P.; data curation, S.C., E.P., A.T., W.O., M.-B.C. and F.C.; writing—original draft preparation, S.C. and F.C.; writing—review and editing, S.C., E.P., A.T., W.O., M.-B.C. and F.C.; visualization, S.C., E.P., A.T., W.O., M.-B.C. and F.C.; supervision, S.C. and F.C.; project administration, S.C. and F.C. All authors have read and agreed to the published version of the manuscript.

Funding: This research was partially carried out within the MICS (Made in Italy—Circular and Sustainable) Extended Partnership and received partial funding from the European Union Next-Generation EU (Piano Nazionale Di Ripresa E Resilienza (PNRR)—Missione 4 Componente 2, Investimento 1.3—D.D. 1551.11-10-2022, PE00000004).

Institutional Review Board Statement: Not applicable.

Informed Consent Statement: Not applicable.

Data Availability Statement: The original contributions in this study are presented in the article/Supplementary Material; further inquiries can be directed to the corresponding author.

Conflicts of Interest: The authors declare no conflict of interest.

References

1. Taviot-Guého, C.; Prévot, V.; Forano, C.; Renaudin, G.; Mousty, C.; Leroux, F. Tailoring Hybrid Layered Double Hydroxides for the Development of Innovative Applications. *Adv. Funct. Mater.* **2018**, *28*, 1703868. [[CrossRef](#)]
2. Khalili, L.; Dehghan, G.; Fazli, A.; Khataee, A. State-of-the-Art Advancement of Surface Functionalized Layered Double Hydroxides for Cell-Specific Targeting of Therapeutics. *Adv. Colloid. Interface Sci.* **2023**, *314*, 102869. [[CrossRef](#)] [[PubMed](#)]
3. Kumari, S.; Sharma, V.; Soni, S.; Sharma, A.; Thakur, A.; Kumar, S.; Dhama, K.; Sharma, A.K.; Bhatia, S.K. Layered Double Hydroxides and Their Tailored Hybrids/Composites: Progressive Trends for Delivery of Natural/Synthetic-Drug/Cosmetic Biomolecules. *Environ. Res.* **2023**, *238*, 117171. [[CrossRef](#)] [[PubMed](#)]
4. Kovalenko, V.; Kotok, V.; Murashevych, B. Layered Double Hydroxides as the Unique Product of Target Ionic Construction for Energy, Chemical, Foods, Cosmetics, Medicine and Ecology Applications. *Chem. Rec.* **2024**, *24*, e202300260. [[CrossRef](#)] [[PubMed](#)]
5. Ameena Shirin, V.K.; Sankar, R.; Johnson, A.P.; Gangadharappa, H.V.; Pramod, K. Advanced Drug Delivery Applications of Layered Double Hydroxide. *J. Control Release* **2021**, *330*, 398–426. [[CrossRef](#)] [[PubMed](#)]
6. Carazo, E.; Borrego-Sánchez, A.; García-Villén, F.; Sánchez-Espejo, R.; Cerezo, P.; Aguzzi, C.; Viseras, C. Advanced Inorganic Nanosystems for Skin Drug Delivery. *Chem. Rec.* **2018**, *18*, 891–899. [[CrossRef](#)] [[PubMed](#)]
7. Chaillot, D.; Bennici, S.; Brendlé, J. Layered Double Hydroxides and LDH-Derived Materials in Chosen Environmental Applications: A Review. *Environ. Sci. Pollut. Res.* **2021**, *28*, 24375–24405. [[CrossRef](#)]
8. Mishra, G.; Dash, B.; Pandey, S. Layered Double Hydroxides: A Brief Review from Fundamentals to Application as Evolving Biomaterials. *Appl. Clay Sci.* **2018**, *153*, 172–186. [[CrossRef](#)]

9. Kuthati, Y.; Kankala, R.K.; Lee, C.H. Layered Double Hydroxide Nanoparticles for Biomedical Applications: Current Status and Recent Prospects. *Appl. Clay Sci.* **2015**, *112–113*, 100–116. [[CrossRef](#)]
10. Kesavan Pillai, S.; Kleyi, P.; de Beer, M.; Mudaly, P. Layered Double Hydroxides: An Advanced Encapsulation and Delivery System for Cosmetic Ingredients—an Overview. *Appl. Clay Sci.* **2020**, *199*, 105868. [[CrossRef](#)]
11. Perioli, L.; Sisani, M. Veicolazione Di Acido Azelaico Con Argille Anioniche in Prodotti Cosmetici. *KOSMETICA* **2013**, *1*, 28–33.
12. Pagano, C.; Perioli, L.; Latterini, L.; Nocchetti, M.; Ceccarini, M.R.; Marani, M.; Ramella, D.; Ricci, M. Folic Acid-Layered Double Hydroxides Hybrids in Skin Formulations: Technological, Photochemical and in Vitro Cytotoxicity on Human Keratinocytes and Fibroblasts. *Appl. Clay Sci.* **2019**, *168*, 382–395. [[CrossRef](#)]
13. Bastianini, M.; Faffa, C.; Sisani, M.; Petracci, A. Caffeic Acid-Layered Double Hydroxide Hybrid: A New Raw Material for Cosmetic Applications. *Cosmetics* **2018**, *5*, 51. [[CrossRef](#)]
14. Rossi, C.; Schoubben, A.; Ricci, M.; Perioli, L.; Ambrogi, V.; Latterini, L.; Aloisi, G.G.; Rossi, A. Intercalation of the Radical Scavenger Ferulic Acid in Hydrotalcite-like Anionic Clays. *Int. J. Pharm.* **2005**, *295*, 47–55. [[CrossRef](#)] [[PubMed](#)]
15. Lima, E.; Flores, J.; Cruz, A.S.; Leyva-Gómez, G.; Krötzsch, E. Controlled Release of Ferulic Acid from a Hybrid Hydrotalcite and Its Application as an Antioxidant for Human Fibroblasts. *Microporous Mesoporous Mater.* **2013**, *181*, 1–7. [[CrossRef](#)]
16. Hashim, N.; Sharif, S.N.M.; Muda, Z.; Md Isa, I.; Ali, N.M.; Bakar, S.A.; Sidik, S.M.; Hussein, M.Z. Preparation of Zinc Layered Hydroxide-Ferulate and Coated Zinc Layered Hydroxide-Ferulate Nanocomposites for Controlled Release of Ferulic Acid. *Mater. Res. Innov.* **2019**, *23*, 233–245. [[CrossRef](#)]
17. Saito, G.P.; Romero, J.H.S.; Cebim, M.A.; Davolos, M.R. Eu(III) Doped LDH Intercalated with Cinnamate Anion as Multifunctional Sunscreens. *J. Lumin.* **2018**, *203*, 160–164. [[CrossRef](#)]
18. Coelho, C.; Hennous, M.; Verney, V.; Leroux, F. Functionalisation of Polybutylene Succinate Nanocomposites: From Structure to Reinforcement of UV-Absorbing and Mechanical Properties. *RSC Adv.* **2012**, *2*, 5430–5438. [[CrossRef](#)]
19. Turcov, D.; Barna, S.; Profire, L.; Iacob, A.T.; Lisă, G.; Puițel, A.C.; Zbranca, A.; Șuteu, D. Physico-chemical characterization of the antioxidant mixture resveratrol-ferulic acid for applications in dermato-cosmetic products. *Farmacia* **2022**, *70*, 410–416. [[CrossRef](#)]
20. Kim, G.D.; Park, Y.S.; Jin, Y.H.; Park, C.S. Production and Applications of Rosmarinic Acid and Structurally Related Compounds. *Appl. Microbiol. Biotechnol.* **2015**, *99*, 2083–2092. [[CrossRef](#)]
21. Marche, A.S.; Vasileva, L.V.; Amirova, K.M.; Savova, M.S.; Koycheva, I.K.; Balcheva-Sivenova, Z.P.; Vasileva, S.M.; Georgiev, M.I. Rosmarinic Acid—From Bench to Valuable Applications in Food Industry. *Trends Food Sci. Technol.* **2021**, *117*, 182–193. [[CrossRef](#)]
22. Amoah, S.K.S.; Sandjo, L.P.; Kratz, J.M.; Biavatti, M.W. Rosmarinic Acid—Pharmaceutical and Clinical Aspects. *Planta Med.* **2016**, *82*, 388–406. [[CrossRef](#)] [[PubMed](#)]
23. Coiai, S.; Cicogna, F.; Pinna, S.; Spiniello, R.; Onor, M.; Oberhauser, W.; Coltelli, M.B.; Passaglia, E. Antibacterial LDPE-Based Nanocomposites with Salicylic and Rosmarinic Acid-Modified Layered Double Hydroxides. *Appl. Clay Sci.* **2021**, *214*, 106276. [[CrossRef](#)]
24. Cicogna, F.; Passaglia, E.; Benedettini, M.; Oberhauser, W.; Ishak, R.; Signori, F.; Coiai, S. Rosmarinic and Glycyrrhetic Acid-Modified Layered Double Hydroxides as Functional Additives for Poly(Lactic Acid)/Poly(Butylene Succinate) Blends. *Molecules* **2023**, *28*, 347. [[CrossRef](#)] [[PubMed](#)]
25. Cicogna, F.; Passaglia, E.; Telleschi, A.; Oberhauser, W.; Coltelli, M.B.; Panariello, L.; Gigante, V.; Coiai, S. New Functional Bionanocomposites by Combining Hybrid Host-Guest Systems with a Fully Biobased Poly(Lactic Acid)/Poly(Butylene Succinate-Co-Adipate) (PLA/PBSA) Binary Blend. *J. Funct. Biomater.* **2023**, *14*, 549. [[CrossRef](#)] [[PubMed](#)]
26. Kowalska, A.; Kalinowska-Lis, U. 18 β -Glycyrrhetic Acid: Its Core Biological Properties and Dermatological Applications. *Int. J. Cosmet. Sci.* **2019**, *41*, 325–331. [[CrossRef](#)] [[PubMed](#)]
27. Coltelli, M.B.; Morganti, P.; Castelvetro, V.; Lazzeri, A.; Danti, S.; Benjelloun-Mlayah, B.; Gagliardini, A.; Fusco, A.; Donnarumma, G. Chitin Nanofibril-Nanolignin Complexes as Carriers of Functional Molecules for Skin Contact Applications. *Nanomaterials* **2022**, *12*, 1295. [[CrossRef](#)] [[PubMed](#)]
28. Panariello, L.; Vannozzi, A.; Morganti, P.; Coltelli, M.B.; Lazzeri, A. Biobased and Eco-Compatible Beauty Films Coated with Chitin Nanofibrils, Nanolignin and Vitamin e. *Cosmetics* **2021**, *8*, 27. [[CrossRef](#)]
29. Coltelli, M.B.; Danti, S.; de Clerk, K.; Lazzeri, A.; Morganti, P. Pullulan for Advanced Sustainable Body- and Skin-Contact Applications. *J. Funct. Biomater.* **2020**, *11*, 20. [[CrossRef](#)]
30. Teno, J.; Pardo-Figuerez, M.; Hummel, N.; Bonin, V.; Fusco, A.; Ricci, C.; Donnarumma, G.; Coltelli, M.B.; Danti, S.; Lagaron, J.M. Preliminary Studies on an Innovative Bioactive Skin Soluble Beauty Mask Made by Combining Electrospinning and Dry Powder Impregnation. *Cosmetics* **2020**, *7*, 96. [[CrossRef](#)]
31. Darvishi, B.; Manoochehri, S.; Kamalinia, G.; Samadi, N.; Amini, M.; Mostafavi, S.H.; Maghazei, S.; Atyabi, F.; Dinarvand, R. Preparation and Antibacterial Activity Evaluation of 18- β -Glycyrrhetic Acid Loaded PLGA Nanoparticles. *Iran. J. Pharm. Res. IJPR* **2015**, *14*, 373–383. [[PubMed](#)]
32. Franco, J.G.; Ataide, J.A.; Ferreira, A.H.P.; Mazzola, P.G. Lamellar Compounds Intercalated with Anions with Solar Protection Function: A Review. *J. Drug Deliv. Sci. Technol.* **2020**, *59*, 101869. [[CrossRef](#)]
33. Wu, J.; Lu, J.; Hu, J.; Gao, Y.; Ma, Q.; Ju, Y. Self-Assembly of Sodium Glycyrrhetinate into a Hydrogel: Characterisation and Properties. *RSC Adv.* **2013**, *3*, 24906–24909. [[CrossRef](#)]
34. Chevolleau, S.; Mallet, J.F.; Ucciani, E.; Gamisans, J.; Gruber, M. Antioxidant Activity in Leaves of Some Mediterranean Plants. *J. Am. Oil Chem. Soc.* **1992**, *69*, 1269–1271. [[CrossRef](#)]

35. Koleva, I.I.; Van Beek, T.A.; Linssen, J.P.H.; De Groot, A.; Evstatieva, L.N. Screening of Plant Extracts for Antioxidant Activity: A Comparative Study on Three Testing Methods. *Phytochem. Anal.* **2002**, *13*, 8–17. [[CrossRef](#)] [[PubMed](#)]
36. Kalinowska, M.; Piekut, J.; Bruss, A.; Follet, C.; Sienkiewicz-Gromiuk, J.; Świsłocka, R.; Rzączyńska, Z.; Lewandowski, W. Spectroscopic (FT-IR, FT-Raman, ¹H, ¹³C NMR, UV/VIS), Thermogravimetric and Antimicrobial Studies of Ca(II), Mn(II), Cu(II), Zn(II) and Cd(II) Complexes of Ferulic Acid. *Spectrochim. Acta A Mol. Biomol. Spectrosc.* **2014**, *122*, 631–638. [[CrossRef](#)] [[PubMed](#)]
37. Sousa, R.; Da Silva, B.J.M.; Dias, A.A.; Meneses, C.C.F.; Bentes, B.A.; Silva, E.O.; Remédios, C.M.R.; Feio, W.P.; Masson, O.; Alves, C.N.; et al. Ferulate Anion Intercalated into Zn/Al Layered Double Hydroxide: A Promising Intercalation Compound for Inhibition of *Leishmania* (L.) Amazonensis. *J. Braz. Chem. Soc.* **2019**, *30*, 1178–1188. [[CrossRef](#)]
38. Sutton, C.C.R.; Da Silva, G.; Franks, G.V. Modeling the IR Spectra of Aqueous Metal Carboxylate Complexes: Correlation between Bonding Geometry and Stretching Mode Wavenumber Shifts. *Chem. Eur. J.* **2015**, *21*, 6801–6805. [[CrossRef](#)] [[PubMed](#)]
39. Deacon, G.B.; Phillips, R.J. Relationships between the carbon-oxygen stretching frequencies of carboxylate complexes and the type of carboxylate coordination. *Coord. Chem. Rev.* **1980**, *33*, 227–250. [[CrossRef](#)]
40. Saito, G.P.; Matsumoto, A.C.L.; Assis, R.P.; Brunetti, I.L.; Cebim, M.A.; Davolos, M.R. Zn(Ferulate)-Lsh Systems as Multifunctional Filters. *Molecules* **2021**, *26*, 2349. [[CrossRef](#)]
41. Kang, H.; Kim, H.J.; Yang, J.H.; Kim, T.H.; Choi, G.; Paek, S.M.; Choi, A.J.; Choy, J.H.; Oh, J.M. Intracrystalline Structure and Release Pattern of Ferulic Acid Intercalated into Layered Double Hydroxide through Various Synthesis Routes. *Appl. Clay Sci.* **2015**, *112–113*, 32–39. [[CrossRef](#)]
42. Miyagusuku-Cruzado, G.; García-Cano, I.; Rocha-Mendoza, D.; Jiménez-Flores, R.; Giusti, M.M. Monitoring Hydroxycinnamic Acid Decarboxylation by Lactic Acid Bacteria Using High-Throughput UV-Vis Spectroscopy. *Molecules* **2020**, *25*, 3142. [[CrossRef](#)] [[PubMed](#)]
43. Świsłocka, R.; Regulska, E.; Karpinska, J.; Swiderski, G.; Lewandowski, W. Molecular Structure and Antioxidant Properties of Alkali Metal Salts of Rosmarinic Acid. Experimental and DFT Studies. *Molecules* **2019**, *24*, 2645. [[CrossRef](#)] [[PubMed](#)]
44. Zhou, X.; Iqbal, A.; Li, J.; Liu, C.; Murtaza, A.; Xu, X.; Pan, S.; Hu, W. Changes in Browning Degree and Reducibility of Polyphenols during Autoxidation and Enzymatic Oxidation. *Antioxidants* **2021**, *10*, 1809. [[CrossRef](#)] [[PubMed](#)]
45. Cilliers, J.J.L.; Singleton, V.L. Characterization of the products of nonenzymic autoxidative phenolic reactions in a caffeic acid model system. *J. Agric. Food Chem.* **1991**, *39*, 1298–1303. [[CrossRef](#)]
46. Sánchez-Cortés, S.; García-Ramos, J.V. FT surface-enhanced Raman evidence of the oxidative condensation reactions of caffeic acid in solution and on silver surface. *Appl. Spectrosc.* **2000**, *54*, 230–238. [[CrossRef](#)]
47. Ly, T.N.; Shimoyamada, M.; Yamauchi, R. Isolation and Characterization of Rosmarinic Acid Oligomers in *Celastrus Hindsi* Benth Leaves and Their Antioxidative Activity. *J. Agric. Food Chem.* **2006**, *54*, 3786–3793. [[CrossRef](#)] [[PubMed](#)]
48. Huang, P.P.; Cao, C.Y.; Wei, F.; Sun, Y.B.; Song, W.G. MgAl Layered Double Hydroxides with Chloride and Carbonate Ions as Interlayer Anions for Removal of Arsenic and Fluoride Ions in Water. *RSC Adv.* **2015**, *5*, 10412–10417. [[CrossRef](#)]
49. Terpinč, P.; Abramovič, H. A Kinetic Approach for Evaluation of the Antioxidant Activity of Selected Phenolic Acids. *Food Chem.* **2010**, *121*, 366–371. [[CrossRef](#)]
50. Tepe, B.; Eminagaoglu, O.; Akpulat, H.A.; Aydin, E. Antioxidant Potentials and Rosmarinic Acid Levels of the Methanolic Extracts of *Salvia verticillata* (L.) Subsp. *verticillata* and *S. verticillata* (L.) Subsp. *Amasiaca* (Freyn & Bornm.) Bornm. *Food Chem.* **2007**, *100*, 985–989.

Disclaimer/Publisher's Note: The statements, opinions and data contained in all publications are solely those of the individual author(s) and contributor(s) and not of MDPI and/or the editor(s). MDPI and/or the editor(s) disclaim responsibility for any injury to people or property resulting from any ideas, methods, instructions or products referred to in the content.